Dependence of the Gaussian-Lévy transition on the disorder strength in random lasers

Ravitej Uppu and Sushil Mujumdar*

Nano-optics and Mesoscopic Optics Laboratory, Tata Institute of Fundamental Research, 1 Homi Bhabha Road, Mumbai 400 005, India

(Received 5 September 2012; published 22 January 2013)

We examine the dependence of the Gaussian-Lévy transition in random lasers on the disorder strength, through experimental and theoretical studies. Experiments are performed on samples whose disorder strength varied over almost an order of magnitude. It is found that the Lévy regime is easily accessed under low excitation when the disorder is weak, compared to the energetically expensive transition in strong disorder. Besides, under conditions of weak disorder, the transition energy is mildly dependent on the disorder strength. The Gaussian-Lévy transition also progresses rapidly in weakly scattering samples. In the theoretical investigation, we employ an analytical-numerical method to estimate the parameters of intensity statistics in random lasers. A Monte Carlo simulation is implemented to accurately calculate the excitation region of the random laser, yielding the ℓ_g and the geometric features of this region. The aspect ratio of this pumped region allows us to further analytically calculate the scale parameter $\langle L \rangle$ of a photon diffusing out of the amplifying region, thereby providing the power-law exponent μ, which allows us to trace the Gaussian-Lévy transition. We find an excellent agreement between the experimental and the theoretical results on the Gaussian-Lévy transition with regard to the location and the rate of transition as a function of the disorder strength.

DOI: 10.1103/PhysRevA.87.013822 PACS number(s): 42.55.Zz, 42.25.Dd, 05.40.Fb

I. INTRODUCTION

Random lasers are a class of open, disordered, mesoscopic systems with gain [1,2]. These systems, on a generic note, consist of multiple sites of disorder randomly arranged in an amplifying medium that realize an interplay of multiple scattering and amplification [3,4]. The resulting emission exhibits interesting characteristics that mimic a conventional laser output in certain aspects such as intensity divergence and bandwidth collapse above threshold and, also, coherent emission under certain conditions [5–7]. The fact that these systems are easy to fabricate has been responsible for numerous experimental studies [8–16], motivating several theoretical and numerical investigations [17–23].

One feature where this system differs from a conventional laser is the statistical behavior. The inherent disordered nature of the system implies that the output parameters of this system are probabilistically distributed. In recent years, therefore, a lot of attention has been devoted to studies relevant to statistics of photon number, mode number, frequency spacing, spatial mode extent, etc. [24–29]. A particularly exciting class of statistical phenomena constitutes those that exhibit non-Gaussian statistics. Even in the absence of optical gain, non-Gaussian statistics has been observed from disordered optical systems. For instance, Lévy flights of photons have been reported in specially engineered disordered systems [30]. Non-Gaussian long-tailed behavior of photon dwell times in strongly scattering systems has been demonstrated [31]. In the context of amplifying disordered systems, the power-law behavior manifests in the relative fluctuations of mode number [27] and in intensity fluctuations [32–35,37]. To be specific, Lévy statistics in emission intensity have been predicted using theoretical and numerical considerations [32]. Such behavior has also been experimentally demonstrated in coherent random lasers [33,34]. Low correlations between pump and emission fluctuations—a consequence of Lévy statistics—have been demonstrated in static disorder [35]. An alternative theoretical approach based on the Langevin equation for the energy density field has been proposed to explain the Lévy fluctuations of intensity [36]. Recently, we experimentally investigated and identified the Gaussian-Lévy-Gaussian transition in intensity statistics in coherent random lasers [37]. These experimental observations were in excellent agreement with the theoretical predictions in [32]. Interestingly, the first transition, i.e., the Gaussian-Lévy transition (GLT) appeared to be insensitive to the disorder strength, a feature which deserves closer examination and is treated in this article.

Intensity fluctuations in random lasers follow an asymptotic power-law behavior due to the underlying distributions in the complex system [32,38]. The amplification incurred by a photon is exponentially proportional to the path length it covers before exiting the boundaries, called the first-passage length. These lengths follow an exponentially decaying distribution. The asymptotic decay of the intensity distribution then follows a power-law with a non-negative exponent, $1 + \mu$, such that $\mu = \frac{\ell_g}{\langle L \rangle}$, where ℓ_g (the gain length) is the length over which one photon amplifies to two, and $\langle L \rangle$ is the scale parameter of the first-passage length distribution. The behavior is Lévy for $0 < \mu < 2$ and Gaussian otherwise. Thus, the parameter μ is a vital quantity that determines the statistical behavior of the random laser system, and it is desirable to develop theoretical techniques to estimate the same. In a complex system such as the random laser, seemingly independent parameters such as ℓ_g and ℓ_s are actually interdependent because the gain realized in a system depends upon the incoupled excitation, which is determined by the disorder strength. Naturally, an intricate dependence of the transition on the disorder strength can be expected to be built in the system. In this paper, we address the disorder dependence of the GLT via experimental and theoretical means. First, we describe experimental data obtained over a large range of

*mujumdar@tifr.res.in; http://www.tifr.res.in/~mujumdar

 ©2013 American Physical Society

disorder, where a clear dependence of the GLT on the degree of disorder was observed. Next, we examine the underlying physics of this dependence using theoretical and numerical techniques to estimate the GLT. An analytical method that computes first-passage lengths of photons is complemented with a numerical Monte Carlo (MC) technique that invokes realistic disorder and amplification conditions. Lévy exponents μ are thus generated for a large range of gain and disorder, which elucidates the disorder dependence of the transition. The study shows that low pump energies are sufficient to take the weakly scattering samples into the Lévy regime. The dependence of the GLT and the rate of the transition on disorder strength are reproduced by the analysis. We find an excellent agreement between the experimental observations and the theoretical conclusions.

This paper is arranged as follows. Section II discusses the results of experimental investigations carried out over a wide range of disorder. Section III describes the calculation of the first-passage times (FPTs) of photons in a cylindrical volume. The required geometrical parameters of the cylinder are obtained in Sec. IV using an MC simulation that calculates the excitation volume of a random laser system. Finally, Sec. V presents the results of the analysis and a comparison with experimental data.

II. EXPERIMENTAL STUDIES

In our earlier experimental studies on statistical regimes [37], attention was focused on confirming Lévy statistics and identifying the statistical transitions. The strength of disorder (quantified by the scattering mean free path ℓ_s, which is the mean separation between two scattering centers) was varied from $\ell_s = 1.3$ mm up to $\ell_s = 2.4$ mm, a range over which the experimental data indicated an apparent insensitivity to the disorder. To re-examine this behavior, we carried out experiments over a larger range of disorder, namely, from 250 to 1475 μm, i.e., almost an order-of-magnitude variation.

The experimental samples consisted of a suspension of dielectric nanoparticles (ZnO; average size, ~10 nm) in a solution of rhodamine 6G in methanol (concentration, 2.5 mM). Various samples were made, with the mean free path varying over an order of magnitude. Excitation was provided by a pulsed Nd:YAG laser ($\lambda = 532.8$ nm; pulse width, 25 ps) with a focal spot of ~60 μm. The emission from the front face was imaged onto the input slit of a spectrometer ($f = 50$ cm). At each excitation energy, 2000 spectra were grabbed. Two representative spectra, at disorder strengths of $\ell_s = 1475$ μm and $\ell_s = 350$ μm, are shown in Fig. 1. As is now known, the weakly scattering samples exhibit strong coherent modes in the spectra, compared to the stronger samples, where the modes are suppressed. Samples stronger than $\ell_s = 250$ μm barely provided discernible peaks and were not analyzed. The intensity at $\lambda = 557$ nm, which roughly corresponded to the wavelength of peak intensity, was recorded for analysis. The statistical distribution of this intensity set was performed using a Lévy-stable fit [39]. An existing algorithm was utilized to perform the fit, which yielded the tail parameter α [40]. The advantage of this procedure is that it fits the actual data, and not a histogram, which suffers from subjectivity in binning. The magnitude of α defined the regime of intensity

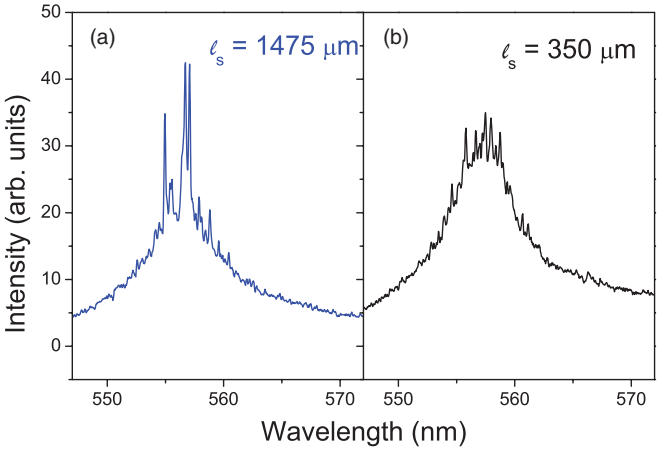

FIG. 1. (Color online) Spectral line shape from a random laser with (a) weak disorder, $\ell_s = 1475$ μm, and (b) strong disorder, $\ell_s = 350$ μm. Strong coherent modes are visible in the weak sample and are subdued in the strongly disordered sample.

statistics, as $\alpha < 2$ indicates Lévy statistics, while $\alpha = 2$ denotes Gaussian statistics. Thus, the GLT is indicated when the α drops to a value below 2, and the excitation energy at which it occurs is the transition energy. Figure 2 shows the transition energy for samples with varying disorder strengths. The inset shows the variation of α with E_p for three samples. For $\ell_s = 1475$ μm [(green) triangles], α drops below 2 at an excitation $E_p < 0.6$ μJ. The same occurs at 0.8 μJ and $\ell_s = 620$ μm [(blue) circles] and at 1.6 μJ and $\ell_s = 350$ μm [(magenta) squares]. These excitation energies are plotted as filled (red) circles in Fig. 2. An interesting variation is observed in the transition energies. Up to a disorder strength weaker than $\ell_s = 620$ μm, the GLT energy varies very gradually, and the variation is almost linear. Despite ℓ_s varying over a range of 800 μm, the excitation energy required for the GLT changes minimally. This weak variation makes the GLT appear

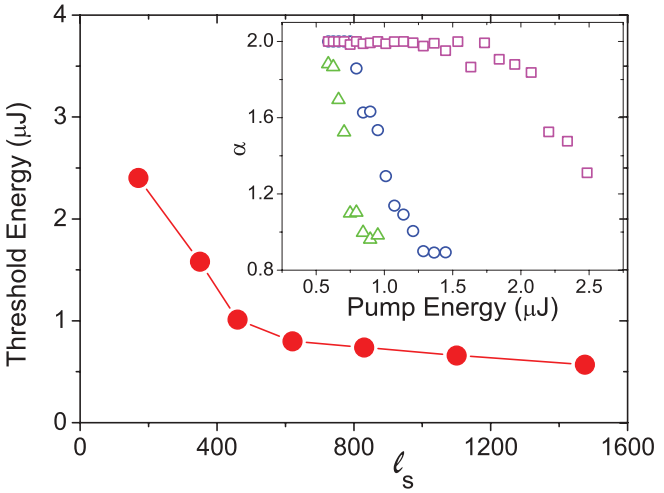

FIG. 2. (Color online) Excitation energy E_p [filled (red) circles] at which the tail exponent α of a Lévy stable fit enters the Lévy domain ($\alpha < 2$), indicating the Gaussian-Lévy transition. (See text for explanation.) Inset: Experimentally observed variation of α with E_p for $\ell_s = 1475$ [(green) triangles], $l_s = 620$ [open (blue) circles], and $l_s = 350$ μm [(magenta) squares].

to be independent of the disorder strength, as reported in our earlier observation. Upon increasing the disorder, beyond the inflection point at $\ell_s = 450\ \mu$m, a strong variation is observed wherein larger increments in excitation energy are required for the GLT. Thus, two scales of variation are seen in the overall plot. A second observation can be made related to the rate of the GLT. The rate, here, describes the propensity of the statistics to transit from the Gaussian to a strong Lévy domain. Qualitatively, the slope of the curve indicates the rate of the transition. The inset in Fig. 2 shows that the weak samples exhibit a rapid transition into the Lévy domain, while the stronger samples exhibit a gradual transition.

Thus, a clear disorder dependence is observed in the GLT. A change in the scale of the dependence suggests that the dynamics of the random lasing system are different in the weak and the strong scattering limits. In order to understand this behavior, we proceeded to theoretically estimate the GLT by calculating the power-law exponent μ in a realistic random laser system, as described in the following sections.

III. FIRST-PASSAGE TIME CALCULATIONS

We apply here the method outlined in [41], wherein the FPTs of diffusing particles through a cylindrical volume were calculated. The technique considers the Green's function form of the diffusion equation

$$\left(\frac{\partial}{\partial\tau} - D\nabla^2\right) G(\vec{r},\tau|\vec{r'}) = \delta(\tau)\delta(\vec{r}-\vec{r'}), \tag{1}$$

where $\tau = t - t'$ is the difference between the observation time t and the source time t' and D is the diffusion coefficient.

After rescaling all lengths by L and all times by L^2/D, the Laplace transformation with respect to τ is

$$(s - \nabla^2)\hat{G}(\vec{r},s|\vec{r'}) = \delta(\vec{r}-\vec{r'}). \tag{2}$$

In the random laser scenario, the motivation to use a cylindrical geometry $[\vec{r} = (\rho,z,\phi)]$ stems from the geometry of the excitation region, as discussed later. In the rescaled coordinates, the ends of the cylinder are located at $z = 0$ and $z = 1$ and the cylinder wall is at $\rho = 1/\beta$, where $\beta = L/a$ is the aspect ratio of a cylinder of length L and radius a. The solution to the equation in the Laplace domain provides the particle currents $\hat{j}_0$ and $\hat{j}_1$ through the front and the back face, respectively. The "particles" here are the spontaneously emitted photons, released by the de-excitation of the molecules of the amplifying medium. The Laplace transform of the current $[\hat{j}_i(s|\vec{r'})]$ yields the splitting probability π_0 and π_1, which are the conditional probabilities that the photon exits the front face and the back face, respectively. Since the spontaneously emitted photon is equiprobable to travel in any direction, the π_i values are not biased.

Finally, the splitting probabilities and the mean- FPT work out to be [41]

$$\pi_0(\vec{r'}) = 2\sum_{n=1}^{\infty} \frac{\operatorname{csch}(x_{0n}\beta)}{x_{0n}J_1(x_{0n})} J_0(x_{0n}\beta\rho') \sinh[x_{0n}\beta(1-z')], \tag{3}$$

$$\pi_1(\vec{r'}) = 2\sum_{n=1}^{\infty} \frac{\operatorname{csch}(x_{0n}\beta)}{x_{0n}J_1(x_{0n})} J_0(x_{0n}\beta\rho') \sinh(x_{0n}\beta z'), \tag{4}$$

$$\langle\tau_0(\vec{r'})\rangle = \frac{1}{\pi_0(\vec{r'})\beta} \sum_{n=1}^{\infty} \frac{\operatorname{csch}(x_{0n}\beta)}{x_{0n}^2 J_1(x_{0n})} J_0(x_{0n}\beta\rho') \times\{\coth(x_{0n}\beta)\sinh(x_{0n}\beta z') - (1-z') \times\cosh[x_{0n}\beta(1-z')]\}, \tag{5}$$

where x_{0n} is the nth 0 of the zeroth-order Bessel function of the first kind, J_0.

This expression computes the $\langle\tau(\vec{r'})\rangle$ as a function of the starting position $\vec{r'}$ of the photon. In the scenario of the random laser, the photons are released at a position determined by the distribution of the excited population. Thus, the first-passage lengths can be estimated by obtaining the geometrical details of the pumped volume and the distribution of the excited population. The $\langle L\rangle$ can then be obtained as $v\langle\tau_0\rangle$.

To obtain an estimate of these parameters for an experimentally realistic system, we employ the MC method of photon transport to simulate the excitation process of the random laser. The MC technique simulates an instantaneous inversion of the system, which is equivalent to the experimental implementation of picosecond pumping since the conventionally used amplifying media decay over nanosecond time scales. This situation can be accurately modeled by the MC simulation. This also facilitates comparison of results from experiments obtained under picosecond pumping, as discussed in this paper.

IV. MONTE CARLO SIMULATIONS

The simulation computes the propagation of light in terms of multiply scattered photon paths, coupled with concurrent absorption. Here, we describe the essentials of the simulation, and the reader is directed to further technical details in [7] and [19]. The MC simulation assumes the random laser system to be in a virtual box; for this study, it was of dimensions $1 \times 1 \times 3$ mm. Disorder is simulated by assuming an ensemble of spherical scatterers randomly distributed in the box. The number density and size parameter of the scatterers yield the mean free path ℓ_s of light. An amplifying medium is assumed to occupy the interscatterer region; in this case, it is a 2.5 mM solution of rhodamine 6G in methanol. It is characterized by the absorption cross section of rhodamine 6G. The excitation of the sample is simulated as follows. An ensemble of pump photons ($\lambda = 532$ nm) is launched from the front face of the box, with initial angular coordinates $(\theta_0,\phi_0) = (0,0)$, thus creating a trajectory perpendicular to the face. The spatial distribution of the photons is assumed to be a Gaussian with a 60-μm width, simulating a laser-beam spot of the said diameter. Each photon carries a weight w at the time of launch. Subsequent to entering the front face, each photon undergoes a three-dimensional random walk throughout the volume. The discrete walk is essentially a set of connected rectilinear paths, with lengths ℓ picked up from an exponential distribution with mean ℓ_s. At the end of the ith path, the photon is propelled into another direction (θ_i,ϕ_i), uniformly distributed over 4π. The excitation of the sample happens via the attenuation of the photon weight, which is determined by the absorption length of the rhodamine molecules and their ground-state population $\ell_{\text{abs}} = [N_0\sigma_{\text{abs}}(\lambda)]^{-1}$. Concurrent with the attenuation of w, a proportional number of ground-state molecules are locally raised to the excited state. Finally, the walk terminates when

either the photon is completely absorbed ($w < 1$) or it exits the box. The desired magnitude of excitation energy determines the total number of photons to be simulated. The excitation leads to local population inversion, which is recorded in a three-dimensional grid, with resolution $2 \times 2 \times 2$ μm. The recorded inversion provides the requisite geometric details of the excitation subvolume.

V. RESULTS

Figure 3 describes the properties of the excited region as calculated from the simulation. The transverse snapshots of the excitation region at an excitation energy of 4.5 μJ for three scattering strengths—namely, $\ell_s = 100$ μm, $\ell_s = 300$ μm, and $\ell_s = 1500$ μm—are depicted in Fig. 1(a). The color bar is in logarithmic scale. The longitudinal extent of the excitation region decreases with increasing scattering, while the transverse dimension increases. The streaky features seen particularly in the weaker sample are a consequence of the discreteness of the MC simulations. The excitation remains axially symmetric and can be best approximated by a cylindrical shape, providing the motivation to study the system in a cylindrical coordinate system. Accordingly, a cylindrical region is chosen for analysis, as represented by the white line in the middle image. The sharp conical termination of the excited region remains excluded in this procedure. Nonetheless, it can

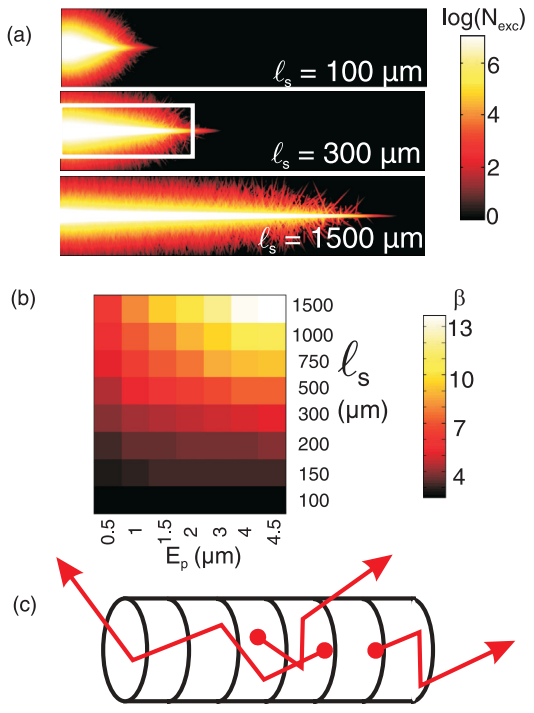

FIG. 3. (Color online) (a) Snapshots of pump distributions for systems with $\ell_s = 100$, 300, and 1500 μm at a pump energy of 4.5 μJ. The color bar indicates the logarithm of the upper-state population. The white rectangle represents the cylindrical region chosen for analysis. (b) Computed aspect ratio (β) of cylindrical excited regions for various ℓ_s and pump energies. (c) Schematic showing representative photon paths exiting the front face, back face, and wall of the cylinder. Only the front-face photons are detected; the others are absorbed.

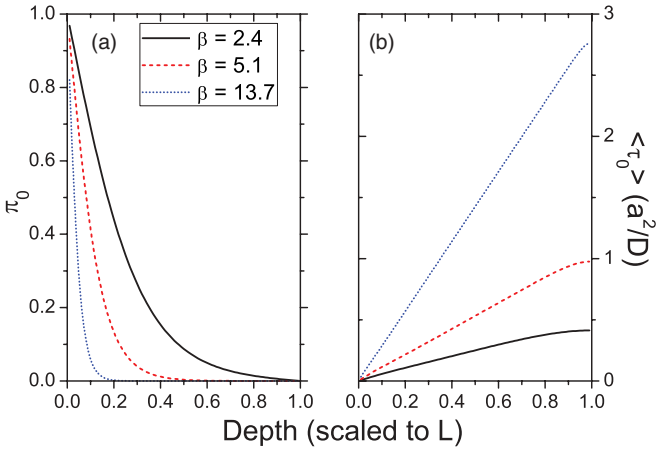

FIG. 4. (Color online) (a) Splitting probability π_0 (exit from front face) as a function of the starting position of photons, for three aspect ratios: $\beta = 2.4$, 5.12, and 13.72. The distribution shows a strong nearest-face bias for large β. (b) Variation of $\langle \tau_0 \rangle$ for the three cases as a function of the starting position.

be expected that the excluded region contributes negligibly to the emission due to the largely unexcited, and hence absorbing, dye. It can be clearly seen that the aspect ratio, the ratio of the longitudinal to the transverse extent, of the excited subvolume varies with ℓ_s. Figure 3(b) illustrates a map the calculated aspect ratios β, which vary from a little under 4 to $\sim$13, for the various values of ℓ_s and pump energies treated in this analysis. The strongest variation is observed under weak scattering and strong pump, evidently because of better incoupling of the excitation energy into the sample. Figure 3(c) shows a schematic of the procedure. Representative photon paths exiting from the front face, the back face, and the cylinder wall are shown. The analysis assumes absorbing boundaries at each wall, out of which the absorbed fraction in the front face would be the photons that are detected in the experiment. The procedure first computes the probability of photons exiting from the front face as a function of the starting position and then calculates the corresponding mean FPTs, as described in Sec. II.

Figure 4(a) shows the splitting probability π_0 as a function of the starting position on the axis of the cylinder. The situations for three aspect ratios, $\beta = 2.4$, 5.1, and 13.7, are discussed. The three correspond to ($\ell_s = 100$ μm, $E_p = 0.5$ μJ), ($\ell_s = 300$ μm, $E_p = 4.5$ μJ), and ($\ell_s = 1500$ μm, $E_p = 4.5$ μJ), respectively. Clearly, for large β, the photons exhibit a large bias to exit to the nearest face. For smaller β, the deeper-generated photons do have a propensity to reach the front face. Figure 4(b) shows the distribution of the FPTs τ_0 that exit from the front face as a function of the starting positions of the photons for the same three systems. This variation remains linear up to a significant depth inside the cylinder. The τ_0 values are of the order of a^2/D. Higher aspect ratios enable longer paths in the excitation region, leading to larger τ_0 values. Interestingly. these first-passage properties have a direct influence on the spectral line shape. In the case of large β, the deeper-born photons with a larger τ_0 gain more in intensity, but very few of them exit from the front face due to the vanishing π_0. These rare photons

create the discrete intense peaks in the spectrum, as shown in Fig. 1(b), which shows the spectrum for a weakly scattering sample. If the β is small, the first-passage properties indicate that many deeper-born photons can reach the detector, but the gain gathered by these photons will only be moderate, due to the small τ_0. Thus, these photons lead to a large number of low-intensity peaks that effectively average out the spectral line shape. This is shown in Fig. 1(a), which shows the spectrum of a strongly scattering sample. Furthermore, the above first-passage properties also shed light on the disorder dependence of the fluctuations. A system with a large β will output photons with a larger range of intensity fluctuations, owing to the large range of $\langle\tau_0\rangle$. On the other hand, this range is smaller for systems with a smaller β. To generate sufficiently fluctuating intensities, the gain needs to be larger, necessitating stronger pumping. Indeed, experiments show that weaker-scattering systems exhibit larger intensity fluctuations than stronger systems at a given excitation energy. These strong fluctuations lead to Lévy statistics. We explicitly calculate ℓ_g, $\langle L\rangle$, and μ to put this qualitative description on a more quantitative footing in the later part of this paper.

At this stage, two issues need to be considered in order to apply this analysis to realistic experimental systems. The first is the modification of starting positions of the photons under anisotropic excitation, and the other is the applicability of diffusion-based analysis to very small system sizes, particularly since Fig. 3 indicates a system size of the order of the ℓ_s, or even smaller. To address these issues, we explicitly simulated the system via MC simulation. MC simulation can also be used for relaxation of the inverted system, and each emitted photon can be tracked for the length distribution [7]. Hence, in principle, the same studies can be implemented purely via the MC simulations. However, these simulations are computationally expensive, and the requirement of the simulation of a huge number of photons can be avoided by techniques such as the one utilized here. For purposes of comparison, we simulate a strong- and a weak-disordered scattering system at $E_p = 4.5$ μJ. The results are depicted in Fig. 5. Black symbols (circles, $\ell_s = 300$ μm; squares, $\ell_s = 1500$ μm) depict the MC results, while solid (red) curves are the calculated data using the above technique. In both situations, the calculated curves accurately reproduce the behavior of the tail, which signifies the long-path photons that comprise the multiply scattered light. This shows that the small but definitive diffusive component in the system is captured by the analysis. This is precisely the component that gathers maximal gain and realizes power-law statistics due to its exponential distribution, as discussed earlier. The early-time component in the MC simulations represents the ballistic light which realizes only modest gain and manifests in deviations from the power-law statistics. Thus, although diffusion theory cannot account for the complete transport in such a system, this analysis does accurately elucidate the parameters of the diffusive fraction. The figure also illustrates the effect of the anisotropic pump distribution. The dashed (blue) curves show the FPT distribution when the starting positions of the photons are uniformly distributed over the entire cylinder. The scale parameters $\langle L\rangle$ in this case are 312 and 278 μm for $\ell_s = 300$ and 1500 μm, respectively. In the experimental scenario, the photon random walks commence at positions of spontaneous

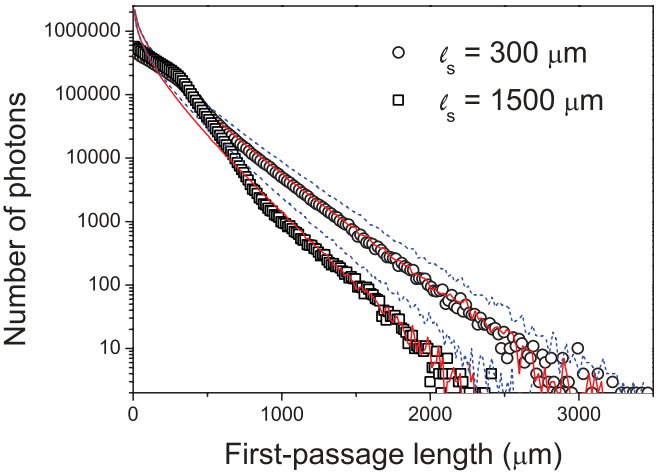

FIG. 5. (Color online) Comparison between the Monte Carlo analysis of random lasing photons (black symbols: circles, $\ell_s = 300$ μm; squares, $\ell_s = 1500$ μm) and the analytical calculation (red solid and blue dashed lines). Dashed (blue) lines show the analytically calculated variation when the starting positions of all photons are uniformly distributed over the cylindrical region. The solid (red) line shows the variation when the starting positions are corrected using the actual pump distribution. The initial early-time output deviates from the tail and is comprised of ballistic light that does not manifest power-law statistics.

emission which obey the distribution of the gain. Indeed, the solid (red) curves, which are corrected for the starting position, accurately reproduce the MC results, wherein the modified scale parameters are 244 and 190 μm, respectively. Evidently, the weaker samples incur larger corrections in the $\langle L\rangle$ compared to the stronger samples.

The ℓ_g are calculated in a mean-field approach by invoking the upper- and ground-state populations (N_1 and N_2, respectively) as recorded by the MC simulations and the known emission and absorption cross sections for a certain emission wavelength $\lambda = 557$ nm. Thus, $\ell_g = [N_1\sigma_{\rm emm}(\lambda) - N_0\sigma_{\rm abs}(\lambda)]^{-1}$. Figure 6 exhibits the scale parameters $\langle L\rangle$ of the

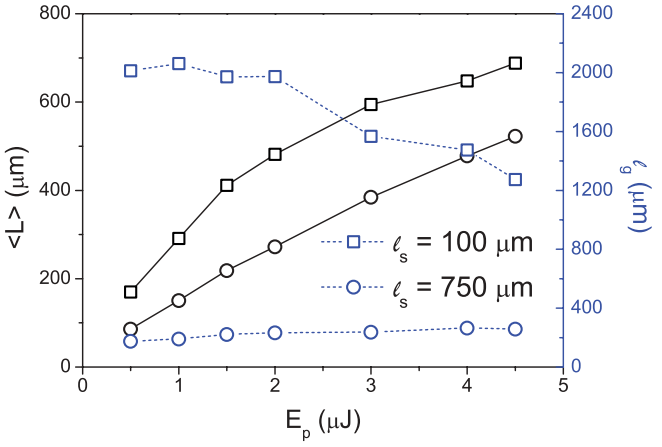

FIG. 6. (Color online) Computed mean first-passage lengths $\langle L\rangle$ [solid (black) curves] and ℓ_g [dashed (blue) curves; right % axis] as a function of pump energy E_p for strong ($\ell_s = 100$ μm; squares) and weak ($\ell_s = 750$ μm; circles) scattering.

first-passage length distributions and the ℓ_g for two scattering strengths. Note that, when the complete range of abscissas is spanned by the distribution ($0 < L < \infty$), the scale parameter equals the inverse mean of the distribution. In the present context, the range of L is strictly limited by the sample size. Black symbols show the $\langle L \rangle$ varying with pump energy, for $\ell_s = 100$ and 750 μm. For the weaker sample, $\langle L \rangle$ increases linearly with E_p, while the stronger sample shows a sublinear rise. Importantly, the magnitude of $\langle L \rangle$ remains smaller than that of ℓ_s over the entire range of E_p for the weaker sample. This is a consequence of the low exit probability through the front face of photons released deeper in the sample, which contribute to the observed data in the experiments. In contrast, $\langle L \rangle > \ell_s$ for the stronger-scattering sample. The two curves can be approximately deduced from the β map shown in Fig. 3(b), which underlines the significance of the size of the system. We found that when the β values are comparable, the $\langle L \rangle$ are proportional to D^{-1}. Thus, the disorder strength determines the size of the pumped subvolume, which, in turn, determines the first-passage properties. The distribution of the excitation energy is also dependent on the ℓ_s, due to which the ℓ_g [shown by dashed (blue) lines] also shows a marked difference between the two samples. For the weaker sample, the ℓ_g is seen to gradually increase with E_p, and it remains small over the entire range of E_p. In the strongly disordered sample, the ℓ_g decreases with pumping and is larger in magnitude compared to ℓ_s over the studied range of E_p.

This behavior has an important bearing on the Lévy character of the statistics. The system is in the Lévy regime when $\ell_g/\langle L \rangle < 2$. At a given excitation, the weak-scattering system allows stronger inversion, which reduces ℓ_g. The $\langle L \rangle$ is large enough to take the system into a Lévy regime. With increasing excitation, the ℓ_g does not change appreciably, but the volume increases, leading to a rise in the $\langle L \rangle$. A strongly disordered environment obstructs the incoupling of the excitation pulse and redistributes it in the sample. This increases the excitation volume while limiting the inversion within, leading to larger ℓ_g compared to the weak sample. With increasing E_p, the increase in volume is slower, so the excitation leads to stronger inversion, lowering the ℓ_g. Although the $\langle L \rangle$ increases with E_p, the increase is rather slow. Therefore, at an appropriately strong excitation, the system enters the Lévy regime.

The subsequently calculated Lévy exponents μ are illustrated in Fig. 7, where the consequences of the above trends are elucidated. The plot depicts μ as a function of the pump energy for eight strengths of disorder ℓ_s, ranging from 100 to 1500 μm. The horizontal dashed (red) line demarcates the lower Lévy region from the upper Gaussian. Evidently, for samples with larger ℓ_s, the exponents are small at weak pumping, indicating the Lévy domain, in contrast to strongly scattering samples. The pump energy required to cross the Gaussian-Lévy domain increases with the disorder strength. The analysis thus shows that the transition from the Gaussian domain into the Lévy domain is easier to attain for samples with weaker scattering, the energy cost for the same being lower than that in the strongly scattering samples. It can be seen that all curves follow the same qualitative behavior. There is an apparent likeness to a power-law function, but

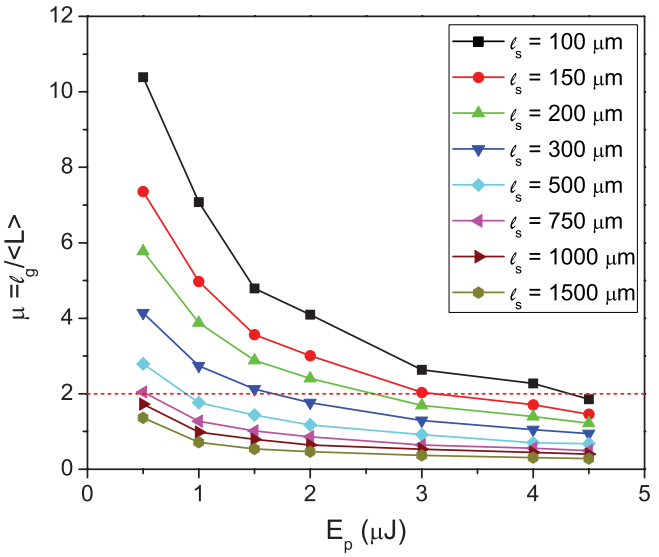

FIG. 7. (Color online) Computed Lévy exponents μ for varying pump energies and ℓ_s. The dashed (red) line separates the Lévy region ($\mu < 2$) from the Gaussian. For stronger scattering, a higher pump energy is required to transit into the Lévy regime. At strong excitation (>2 μJ), all systems are Lévy.

analysis shows a systematic deviation from a power-law behavior.

Figure 8 illustrates a comparison between the theoretically calculated results and the experimental observations. The plot describes the combination of the excitation energy and mean free path at which the random lasing system transgresses from the Gaussian regime to the Lévy regime. In the calculations presented here, this happens when the calculated μ curve for

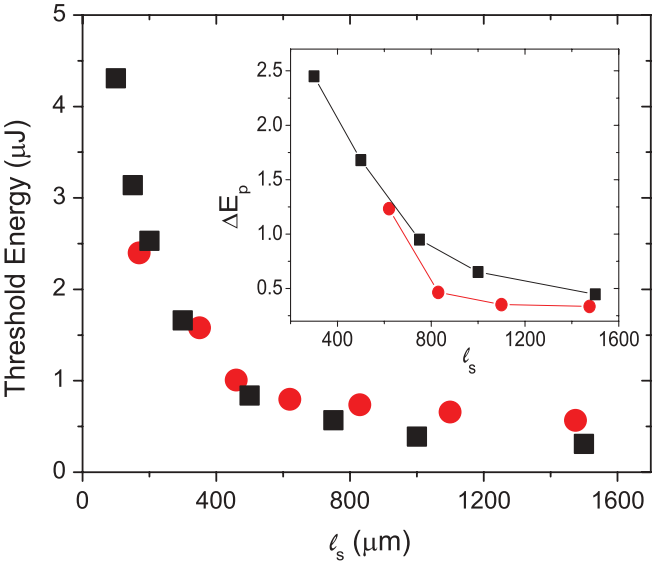

FIG. 8. (Color online) Comparison between the computed trend (squares) for the GLT threshold energy and the experimental observations for various disorder strengths. The same experimental data (circles) as used in Fig. 2, repeated here for easy comparison. Inset: Comparison of the transition rates, where ΔE_p represents the energy range over which α drops from 2 to 1 in the experimental case and μ drops from 2 to 1 in the theoretical case.

the various ℓ_s crosses the $\mu = 2$ line [dashed (red) line] in Fig. 7. These combinations are shown by (black) squares in the plot. It can, indeed, be seen that at weak scattering strengths, the required E_p is small and varies only mildly up to a disorder strength corresponding to $\ell_s = 500$ μm. The weak variation of E_p with ℓ_s creates an apparent insensitivity of the GLT towards the disorder strength, as seen in the earlier experiments. For stronger scattering ($\ell_s < 500$ μm), however, E_p considerably increases with ℓ_s to achieve the GLT, and a different scale of variation can be attributed to this regime of strong scattering. The excellent agreement between the theoretical and the experimental observations is obvious from the plot. The inset in Fig. 8 shows the estimated rate of the GLT. This was calculated as follows. The range of excitation energy ΔE_p over which the exponent (α for experiments and μ for the calculations) falls from 2 to 1 is taken as a quantifiable estimate of the GLT rate. The black curve (squares) shows the calculated increments, which increase with the disorder strengths. This is in qualitative agreement with the experimental observations, depicted by the red curve (circles). In the experiments, the α values did not reach 1 in strong samples, hence the limited points in the curve.

VI. DISCUSSION

In summary, we have addressed the disorder dependence of the GLT in random lasers, using experiments and theoretical studies. We find that weakly scattering systems exhibit Lévy statistics at a lower excitation energy compared to strongly disordered systems. We have presented a theoretical technique to estimate the Lévy exponents in a realistic random laser system. We compute the shape parameters of the excited region of a random laser using a MC technique and further deduce the scale parameter of the first-passage length of a diffusing photon in this region using an analytical technique. The theoretical analysis accurately reproduces the experimental behavior, in terms of the energy of the GLT and its rate. Indeed, the magnitude of excitation energy for the GLT is quantitatively well predicted by the theory, while the transition rates qualitatively agree. Further improvement in the analysis can be attained by improvising the boundary conditions. Random laser systems are open systems, and the effective boundaries are set by the gain. These boundaries are not perfectly absorbing boundaries as treated in this paper but are, rather, soft boundaries wherein transgressing photons may re-enter the active region and participate in the dynamics. The inclusion of such effects may bring the results related to transition rates quantitatively closer to the experimental situation.

The parameters used in this analysis, such as E_p and ℓ_s, were motivated by routine experimental parameters. The observations indicate that samples with large ℓ_s exhibit a Lévy character under low pump. While this trend can theoretically be extrapolated further, such an experimental observation can be challenging. The analysis elucidates that the *existing* diffusive photons in the weakly disordered samples, although small in number, will exhibit Lévy fluctuating intensities. As the ℓ_s increases, the probability of occurrence of the multiply scattered photons falls, as does the exit probability of these photons. In that situation, an excitation pulse may not even realize random lasing. This situation is actually common in experimental studies of coherent random lasing. At energies close to the threshold, it is known that not every pulse realizes ultranarrow modes. Such an effect has actually been used to identify the threshold, by measuring the probability of random lasing [11].

Recent theoretical studies have revealed a rich statistical behavior, wherein the Levy regime of statistics crosses over into a Gaussian regime at a higher excitation energy [32]. This has also been experimentally observed [37]. The trends in Fig. 7 show that μ monotonically decreases with E_p, indicating a transit into the Lévy domain. This trend also continued for higher values of E_p not reported here. Hence, this analysis seems only applicable to a one-way transition, i.e., the statistics can only transit from the Gaussian regime into the Lévy regime with increasing excitation energy. It appears that the physics of the second transition is different from that responsible for the GLT. To explain the second transition, more principles need to be invoked than the mere variation of the two parameters ℓ_g and $\langle L \rangle$. This, however, is outside the scope of this article.

In conclusion, we note that these studies shed light on the interesting statistical GLT in random lasers. We hope that this study will encourage more analysis of non-Gaussian behavior of disordered optical systems. Since diffusion-equation-based analysis is not as computationally expensive as an MC technique, this work can stimulate further theoretical research in these exciting physical systems.

[1] D. S. Wiersma, Nature Phys. **4**, 359 (2008).
[2] H. Cao, J. Phys. A **38**, 10497 (2005).
[3] V. S. Letokhov, Zh. Eksp. Teor. Fiz. **53**, 1442 (1967) [Sov. Phys. JETP **16**, 835 (1968)].
[4] N. M. Lawandy, R. M. Balachandran, A. S. L. Gomes, and E. Sauvain, Nature (London) **368**, 436 (1994).
[5] H. Cao, Y. G. Zhao, S. T. Ho, E. W. Seelig, Q. H. Wang, and R. P. H. Chang, Phys. Rev. Lett. **82**, 2278 (1999).
[6] H. Cao, J. Y. Xu, S.-H. Chang, and S. T. Ho, Phys. Rev. E **61**, 1985 (2000).
[7] S. Mujumdar, M. Ricci, R. Torre, and D. S. Wiersma, Phys. Rev. Lett. **93**, 053903 (2004).
[8] H. E. Türeci, L. Ge, S. Rotter, and A. D. Stone, Science **320**, 643 (2008).
[9] M. Noginov, *Solid State Random Lasers*, Springer Series in Optical Sciences 105 (Springer, New York, 2005).
[10] A. Tulek, R. C. Polson, and Z. V. Vardeny, Nature Phys. **6**, 303 (2010).
[11] J. Fallert, R. J. B. Dietz, J. Sartor, D. Schneider, C. Klingshirn, and H. Kalt, Nature Photon. **3**, 279 (2009).
[12] S. K. Turitsyn, S. A. Babin, A. E. El-Taher, P. Harper, D. V. Churkin, S. I. Kablukov, J. D. Ania-Castañón, V. Karalekas, and E. V. Podivilov, Nature Photon. **4**, 231 (2010).

[13] S. Gottardo, R. Sapienza, P. D. García, A. Blanco, D. S. Wiersma, and C. López, Nature Photon. **2**, 429 (2008).
[14] V. Milner and A. Z. Genack, Phys. Rev. Lett. **94**, 073901 (2005).
[15] S. Mujumdar, V. Turck, R. Torre, and D. S. Wiersma, Phys. Rev. A **76**, 033807 (2007).
[16] R. Uppu and S. Mujumdar, Opt. Lett. **35**, 2831 (2010).
[17] R. Pierrat and R. Carminati, Phys. Rev. A **76**, 023821 (2007).
[18] S. Mujumdar and H. Ramachandran, Opt. Commun. **176**, 31 (2000).
[19] S. Mujumdar, R. Torre, H. Ramachandran, and D. S. Wiersma, J. Nanophoton. **4**, 041550 (2010).
[20] C. Vanneste, P. Sebbah, and H. Cao, Phys. Rev. Lett. **98**, 143902 (2007).
[21] D. S. Wiersma and A. Lagendijk, Phys. Rev. E **54**, 4256 (1996).
[22] P. Pradhan and N. Kumar, Phys. Rev. B **50**, 9644 (1994).
[23] S. John and G. Pang, Phys. Rev. A **54**, 3642 (1996).
[24] C. W. J. Beenakker, J. C. J. Paasschens, and P. W. Brouwer, Phys. Rev. Lett. **76**, 1368 (1996).
[25] H. Cao, Y. Ling, J. Y. Xu, C. Q. Cao, and P. Kumar, Phys. Rev. Lett. **86**, 4524 (2001).
[26] G. Hackenbroich, J. Phys. A **38**, 10537 (2005).
[27] O. Zaitsev, Phys. Rev. A **74**, 063803 (2006).
[28] O. Zaitsev, Phys. Rev. A **76**, 043842 (2007).
[29] K. L. van der Molen, R. W. Tjerkstra, A. P. Mosk, and A. Lagendijk, Phys. Rev. Lett. **98**, 143901 (2007).
[30] P. Barthelemy, J. Bertolotti, and D. S. Wiersma, Nature **453**, 495 (2008).
[31] R. Sapienza, P. Bondareff, R. Pierrat, B. Habert, R. Carminati, and N. F. van Hulst, Phys. Rev. Lett. **106**, 163902 (2011).
[32] S. Lepri, S. Cavalieri, G.-L. Oppo, and D. S. Wiersma, Phys. Rev. A **75**, 063820 (2007).
[33] X. Wu and H. Cao, Phys. Rev. A **77**, 013832 (2008).
[34] D. Sharma, H. Ramachandran, and N. Kumar, Fluct. Noise Lett. **6**, L95 (2006).
[35] G. Zhu, L. Gu, and M. A. Noginov, Phys. Rev. A **85**, 043801 (2012).
[36] S. Lepri, arXiv:1208.5891v1.
[37] R. Uppu, A. K. Tiwari, and S. Mujumdar, Opt. Lett. **37**, 662 (2012).
[38] J.-P. Bouchaud and A. Georges, Phys. Rep. **195**, 127 (1990).
[39] B. V. Gnedenko and A. N. Kolmogorov, *Limit Distributions for Sums of Independent Random Variables* (Addison-Wesley, Reading, MA, 1954).
[40] I. A. Koutrouvelis, J. Am. Stat. Assoc. **75**, 918 (1980).
[41] N. A. Licata and S. W. Grill, Eur. Phys. J. E **30**, 439 (2009).